

Identifying materials limits of chemically amplified photoresists[§]

Wen-li Wu, Vivek M. Prabhu, and Eric K. Lin

Polymers Division, National Institute of Standards and Technology,
Gaithersburg, MD, 20899-8541

Abstract

Chemically amplified photoresists are likely to remain the primary imaging materials for the semiconductor industry. As feature sizes decrease to dimensions comparable to the characteristic size of the molecules in the photoresist, a significant challenge lies in identifying the ultimate resolution limit of these materials. To address this challenge, we investigated model photoresist materials with high resolution measurements to examine the effect of individual factors among interdependent process steps on line-edge roughness (LER). Using a bilayer film sample geometry, we measured the internal deprotection interface with nanometer resolution as a function of photoacid size, initial resist copolymer composition, and amine base quencher by neutron reflectivity and infrared spectroscopy. After development, we found that the resist chemistry and additives can play an important role in LER through its influence on acid diffusion. However, these model experiments suggest that there is a limit in LER even with an idealized exposure image contrast and decreases in the width of the reaction-diffusion front. However, there may be opportunities to further decrease LER during development by tuning the response of the photoresist to the developer solution.

1. Introduction

Line-edge roughness in features fabricated with photolithography can lead to problems in device performance and device yield. This issue is of particular concern with chemically amplified photoresists because they are likely to remain the primary imaging materials for the semiconductor industry. As feature sizes decrease to dimensions comparable to the characteristic size of the molecules in the photoresist, a significant challenge remains in identifying the ultimate resolution limit of these materials. Researchers have worked towards establishing correlations between resist-edge roughness, post-etch roughness, and the resulting parametric data on device performance. However, an important challenge remains in identifying the materials sources LER in the photoresist. If met, lithographers and photoresist designers will understand and be aware of potential limits in the technology and can focus on process steps that provide the best opportunities for LER reduction or to begin work on alternative fabrication strategies.

Identifying the materials limits of chemically amplified photoresists is challenging because of the many interdependent processing and materials variables contributing to LER and the difficulties at examining the lithographic process at current nanometer dimensions. As outlined schematically in Figure 1, LER is a dimensional fluctuation resulting from multiple factors and is strongly process dependent [1]. Besides the properties of photoresist polymer, photoacid generator (PAG), base quencher or other additives, almost all the intermediate procedure play a role on the final LER such as exposure [2-4], post-exposure baking (PEB) [5,6] and development [7-9]. Due to the large number of variables, it is impractical to search for the narrow processing condition windows to optimize a material or process with experiments. General physical and chemical principles that can be utilized to understand specific resist systems are needed because chemically amplified photoresists and aqueous base developers are anticipated for all future wavelengths from 193 nm immersion through EUV (extreme ultraviolet).

[§] Official contribution of the National Institute of Standards and Technology; not subject to copyright in the United States

* Corresponding author. E-mail: vprabhu@nist.gov

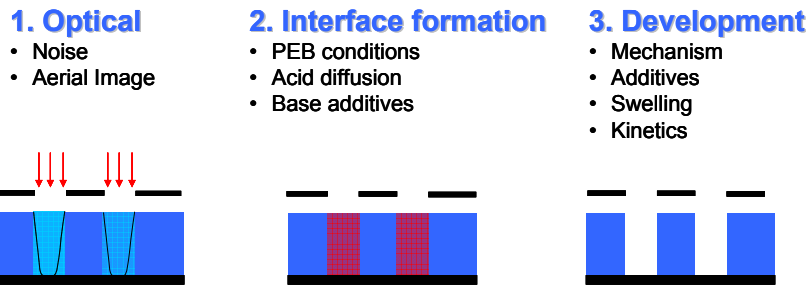


Figure 1. Schematic diagram identifying processes during photolithography with a chemically amplified photoresist that affect the ultimate imaging resolution.

The quality of the final patterned structures is dependent upon factors that influence either the spatial distribution of the photoacid or the spatial extent of the reaction-diffusion process. Using interferometric lithography and varying aerial image contrast, Hinsberg et al. demonstrated that the initial acid catalyst distribution, controlled through the exposure quality, significantly affects the printed feature quality [2]. It has been reported that a relationship between latent image and LER can be established experimentally, in which the LER is dictated by the gradient of deprotection reaction profile [3]. It is found that the LER and the gradient follow master curves. However, these master curves could shift upon changing base quencher concentration or resist polymer type. This finding significantly reduced the parameters to be considered for LER minimization but also led to new questions: what governs this monotonic relationship between LER and the deprotection gradient and what is the source of this deviation? These changes in the feature quality have been correlated with the reaction-diffusion of the photo-generated acid [10-12] into the unexposed regions that leads to image spreading or blurring [13, 14]. Controlling the reaction-diffusion process remains an important strategy for improving feature quality [15-19].

The final step in photolithography is the development process with an aqueous base solution. Numerous approaches have been taken to understand photoresist polymer dissolution through the application of percolation models [20-22], the investigation of interfacial reaction kinetics [23], the development of a surface-etching critical ionization model [24,25], and the combination of reaction kinetics with a critical ionization model [26,27]. However, many ionizable polymers can swell when exposed to an aqueous or aqueous base solution [26]. For these classes of photoresist polymers, the effect of swelling on the rate of dissolution and the influence of the polymer chemistry on swelling remain poorly characterized; swelling may occur for polymers below the entanglement molecular weight and in the absence of chemical cross-links [28-31]. At the line edge with composition below dissolution but active to swell can affect LER. Neutron reflectivity measurements have shown that the line-edge feature remains swollen after development and during the rinse step [32]. Therefore the true surface roughness (or line-edge roughness) is observed only after the deswelling that appears by drying. This work leads to a focused question regarding the resist-chemistry controlling effect to swelling and relationships to the local chemical heterogeneity and LER.

2. Approach

To systematically investigate the relationship between the exposure profile and the reaction-diffusion process, the latent chemical image formation during the reaction-diffusion process in a model 193 nm photoresist system is measured directly with neutron reflectivity and Fourier transform infrared (FTIR) spectroscopy. Then, its relationship to the roughness of the final structure is determined by measuring the surface roughness of the developed film. An idealized step acid profile is prepared by a sequential spin coating process (multilayer). The reaction-diffusion process across this interface occurs during subsequent processing of this ideal optical image. Three ionic photoacid generators are used to measure the reaction front profile resulting from different photoacid size. While the extent of propagation is dependent upon the size of the photoacid, as expected, the profile width also changes. Additionally, the influence of the changing chemical composition on the spatial-extent of the reaction profile can be

clarified. As a point of reference, the “image log-slope” (ILS), a measure of the image contrast at a line-edge, is typically (2 to 25) μm^{-1} . The ILS of the model exposure profile in these experiments is approximately (20 to 400) μm^{-1} . The direct measurement of the reaction-diffusion profile in these experiments provides the insight needed to extend predictive models as well as to select advantageous aspects of this lithographic component.

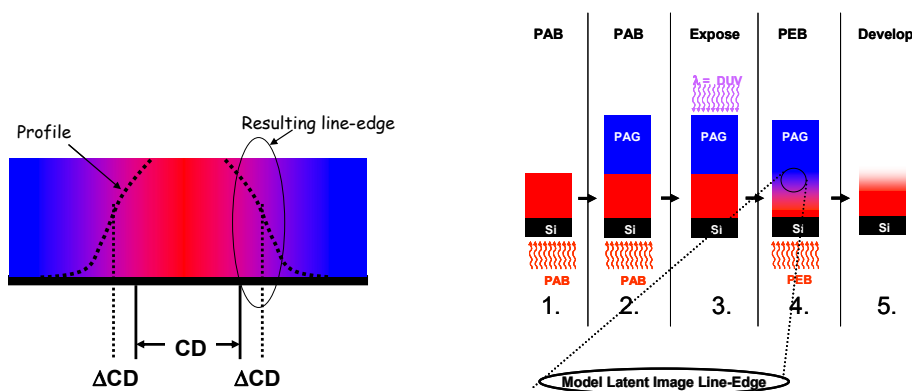


Figure 2. (Left) Schematic diagram of the reaction-diffusion front after exposure during photolithography. (Right) Schematic diagram of the analogous idealized exposure profile with bilayer sample preparation and processing.

3. Experimental⁺

2.1 Model photoresist materials

Three model photoresist polymers based upon poly(methyladamantyl methacrylate) (PMAAdMA) are used. The PMAAdMA homopolymer and a copolymer P(MAdMA41-co-GBLMA59) containing 59 mol% of the non-reactive α -gammabutyrolactone methacrylate (GBLMA) were provided by DuPont Electronics Polymers. A second copolymer containing 50 mol% GBLMA (P(MAdMA50-co-GBLMA50)) was supplied by AZ Electronics. The chemical structures of the polymers are shown in Figure 3. The acid catalyst for the deprotection reaction is produced from a photoacid generator (PAG), triphenylsulfonium perfluorobutanesulfonate (TPS-PFBS), under UV exposure. The photoacid concentration generated from UV was calculated from exposure dose and PAG loading in the sample. The photoacid-catalyzed deprotection reaction is shown in Figure 4. The role of base quencher is examined systematically by adding triethylamine (TOA) selectively to the acid feeder and/or PMAAdMA layers.

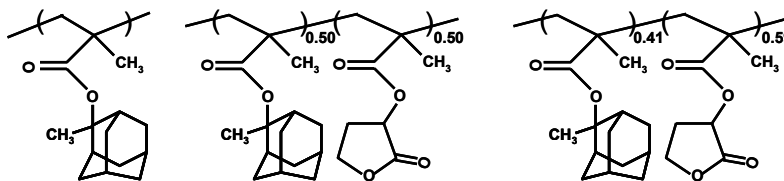


Figure 3. Chemical structures of three photoresists used in this study; Left: PMAAdMA; middle: P(MAdMA50-co-GBLMA50); right: P(MAdMA41-co-GBLMA59).

⁺ Certain equipment, instruments or materials are identified in this paper in order to adequately specify the experimental details. Such identification does not imply recommendation by the National Institute of Standards and Technology nor does it imply the materials are necessarily the best available for the purpose.

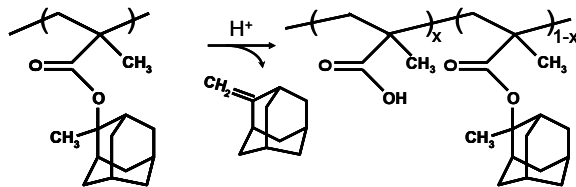


Figure 4. Acid catalyzed deprotection of PMAdMA with methylene adamantane product (MA).

2.2 Model line-edge: Bilayer films

Details on the preparation of bilayer films are provided elsewhere.[34] Films are post apply baked (PAB) at 130 °C to remove residual solvent. The bilayer is exposed to broadband UV radiation (300 mJ/cm²) to activate the PAG. A constant post exposure bake (PEB) temperature of 130 °C is used for the acid-diffusion deprotection reaction. To determine the surface roughness of the bilayers, the acid feeder layer and the deprotected portion of the bottom layer are developed with a 0.26 N tetramethylammonium hydroxide (TMAH) (Aldrich). Different developer strengths were also used to develop the films through dilution of the initial 0.26 N TMAH solution with deionized water.

2.3 Neutron reflectometry

Neutron reflection measurements were performed at the Center for Neutron Research (NCNR) on the NG-7 reflectometer at the National Institute of Standards and Technology (Gaithersburg, MD) in the following configuration: wavelength (λ) = 4.768 Å and wavelength spread ($\Delta\lambda/\lambda$) = 0.025. The large difference in hydrogen content between PHS and PMAdMA allows for the bilayer to be resolved with NR. The hydrogen density of the PMAdMA layer is significantly reduced upon deprotection and loss of methylene adamantane (by-product), thus providing a route for obtaining the deprotection profile through the film thickness. The physical thickness and surface roughness of the films was monitored using x-ray reflectivity (XR) on a Philips X'Pert MRD diffractometer.

2.4 Infrared spectroscopy

Transmission IR spectra were obtained with a Nicolet NEXUS 670 Fourier transform infrared (FTIR) spectrometer and analyzed with OMNIC software. The quantification of deprotection level was based on the CH₃ bending band (1360 cm⁻¹) for PMAdMA and C-O stretching band (1260 cm⁻¹) for the two copolymers. The quantification of MA residual level is based on the stretching vibration of H-C(=C) (3065 cm⁻¹) in the free MA molecule. This band is separated from other H-C(-C) vibration peaks (usually < 3000 cm⁻¹). Since pure MA is not commercially available, the direct calibration from IR absorbance of MA to its molar quantity is not possible. Instead, we use an indirect extrapolation method, where we assume all MA remains in the film when the deprotection or PEB time is close to zero [38].

3. Results and discussion

3.1. Reaction-diffusion front: PAG size and copolymer composition

The effects of photoacid size on the deprotection profile are shown in Figure 5 for a fixed PEB temperature of 130 °C and time of 8 s. The triflic acid propagates completely through the 600 Å PMAdMA film; deprotecting all of the PMAdMA to with extents of reaction greater than 40 %. The acidic proton does not diffuse independently, but is coupled to its conjugate base (e.g., triflate, perfluorobutanesulfonate, or perfluorooctanesulfonate). As the photoacid size is increased from Tf to PFBS, the breadth of the reaction front profile narrows and the propagation depth of deprotection decreases [39]. The sharpest latent image profile is found for PFOS. One concern in the direct comparison between different PAGs at a fixed time is interpreting the photoacid diffusive properties because the activation energy for diffusion in these thin films is dependent upon local compositional environment [34] and the PAG itself. However, Hinsberg et al. found no difference in the activation energy for diffusion between the acid form of Tf and PFBS within a phenolic resist [33]. Thus, we anticipate that observed differences in diffusion between these PAGs are due to the molecular size; not activation energy. It is important to note that the deprotection

profiles in Figure 5 are not photoacid profiles, but represent the image left by the deprotection reaction which follows the reaction kinetics for each photoacid.

A larger PAG imparts a smaller diffusion length thus limiting changes in the critical dimensions and image blur. The shorter diffusion length with increasing PAG size is consistent with previous indirect measurements [33]. When examining the measured deprotection profiles for the case of DTBPI-PFOS, initially at short times, the profile follows an error function, as expected by a diffusive process. However at longer times (> 15 s), the deprotection front almost ceases to propagate, but rather a tail of low deprotection propagates further into the unreacted region (Figure 5). This behavior is consistent with an acid diffusivity that is strongly dependent upon local chemical environment. The PMAA can interact strongly with ionic species, leading to reduced diffusivity similar to that observed for phenolic resists. From a lithographic processing viewpoint, the arrested front is beneficial because the printed dimensions are not strongly dependent upon small variations in PEB time.

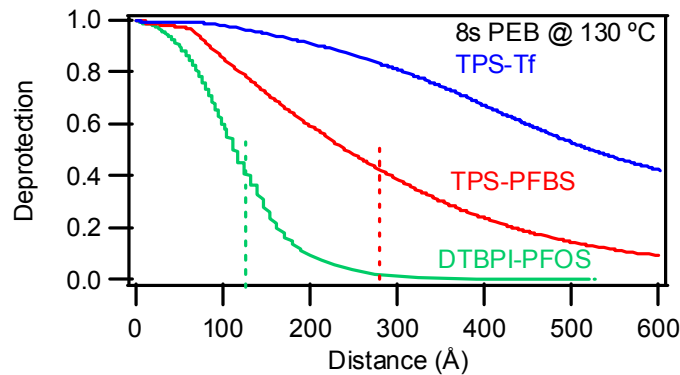


Figure 5. Latent image after PEB of three different PAGs that vary in molecular size. The dashed lines mark where the image is developed in 0.26 TMAH.

These studies have illustrated that the acid diffusion in the deprotected resist is significantly retarded in comparison to its protected analog. Generally, completely different resist systems are examined, so only limited conclusions can be made as to the influence of the polymer composition. The blockiness of the copolymer does not appear to significantly hinder the quality of the printed image, but the hydrophilicity of comonomers has a significant impact. The origins of this dependence have not yet been elucidated. However, the seemingly inert components incorporated as co- or ter-polymers could significantly alter aspects not readily measurable, such as the shape of the deprotection front profile.

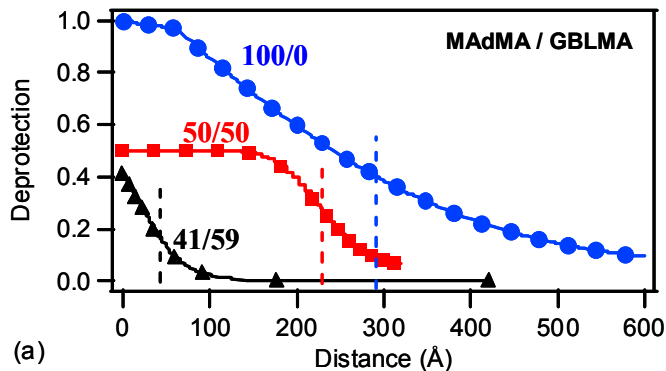


Figure 6. Latent image after PEB of three different photoresist copolymers that vary in composition with an inert monomer group. The dashed lines mark where the image is developed in 0.26 TMAH.

Here we examine the influence of a non-reactive component, α,γ - butyrolactone methacrylate (GBLMA), on the reaction front profile in model 193 nm chemically amplified resists based on poly(methyladamantyl methacrylate) (PMAdMA). Incorporation of lactones in the polymer improves the imaging capabilities of the resist. This group is thought to improve dissolution characteristics through limiting the resist swelling during development. However, the influence of GBLMA on the photoacid diffusion has not been examined in detail. The reaction front profile is measured for two GBLMA contents by combining neutron reflectivity (NR) with Fourier transform infrared spectroscopy (FTIR).

As illustrated in Figure 6, the reaction front profile at the model line edge is sharpened by the addition of GBLMA for 8 s PEB at 130 °C. The change in the shape of the deprotection profile can be attributed to the decrease in the local diffusivity of the photoacid in the vicinity of GBLMA, which will lead to a sharper profile. Previously in examining the reaction kinetics of these resins, the diffusivity of the photoacid, TPS-PFBS, was determined to be an order of magnitude less in GBLMA than in MAdMA.[36] Incorporation of comonomers of GBLMA reduces the initial photoacid diffusivity through the interaction of the acid with the polar GBLMA. Thus, ΔCD would be expected to decrease proportionally to the GBLMA content. At long PEB times, the largest ΔCD is actually found for the intermediate GBLMA composition. Additionally, the reaction-diffusion front ceases to further propagate as illustrated by the plateau in ΔCD .

Simulations by Postnikov et al. also demonstrate this phenomenon [37]. The stochastic nature of the photoacid diffusivity results in some steps back into the reaction front, where the deprotected resist can act to trap the photoacid. Thus as time proceeds there is always a dilution of acid at the front due to trapping. The MAdMA data agree with this model – the dilution of acid at the front leads to a very diffuse profile and ultimately the saturation in ΔCD . The change in the local diffusivity of the photoacid upon deprotection of the MAdMA to MAA as captured by this trapping mechanism and differences in the reaction rates for the copolymers due to changes in local chemical environment are potential sources of the non-monotonic change in ΔCD with GBLMA content.

3.2. Reaction-diffusion front: Effect of base-quencher

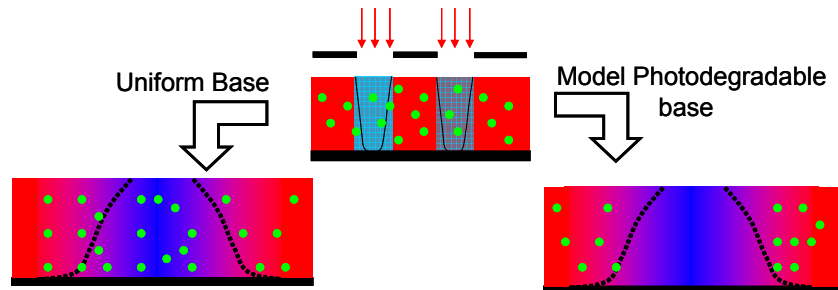


Figure 7. Schematic diagram of two potential locations of a base quencher in a photoresist formulation, a uniform distribution of base or a base that is degraded upon exposure and is eliminated in exposed regions.

Base quenchers are used in photoresist formulations to improve performance by quenching reactions of photoacids that diffuse into unexposed regions [12]. The influence of these neutralizing species on the reaction diffusion process is complex [8]. The quencher appears to partially neutralize the photoacid less than stoichiometrically, influence the dissolution either as promoters or inhibitors, and increase the development induction time. The partial neutralization is consistent with the proportional neutralization model of Houle et al., where the added base initially reduces the amount of acid available after photolysis proportional to the base concentration [8]. Base additives can lead to variation in feature quality, which was attributed to chemical gradients in the resist.

The role of the base quencher can be systematically examined by placement of the amine base in a model bilayer. Generally, the quencher is not photoactive [12] so base would be located uniformly in both exposed (acid feeder layer of the bilayer) and unexposed (protected layer) regions. This case will be compared to a model photodegradable base geometry in which the base is located only in the protected layer.

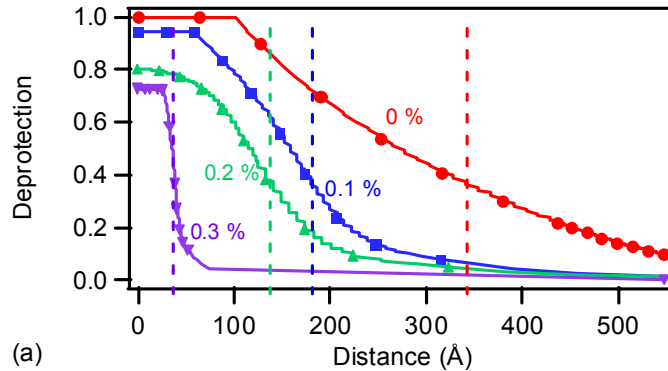


Figure 8. Latent image after PEB with varying levels of base quencher added to both layers uniformly. The dashed lines mark where the image is developed in 0.26 TMAH [40].

The first case examined is for the homogeneous distribution of base; this is analogous to typical resist formulations. As shown in Figure 8, addition of TOA to the bilayer significantly alters the deprotection profile. The MADMA nearest the acid feeder layer is no longer fully deprotected with the addition of TOA and the maximum deprotection decreases with increasing base concentration. Additionally, the penetration depth of the deprotection front is decreased, while the width of the front is sharpened with added TOA.

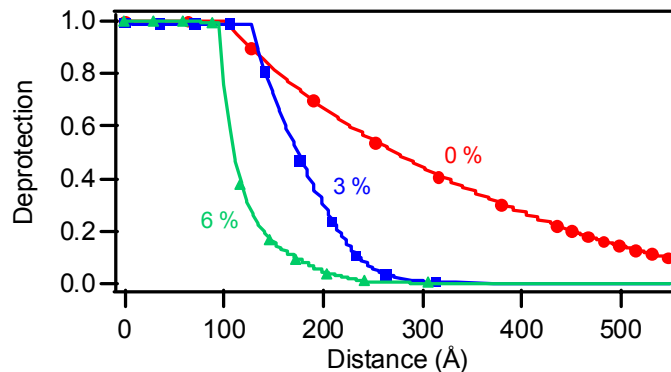


Figure 9. Latent image after PEB with varying levels of base quencher added to the photoresist polymer film only. The dashed lines mark where the image is developed in 0.26 TMAH [40].

The use of photodegradable bases has been proposed to enhance resist sensitivity and potentially limit line edge roughness (LER). To identify the difference between uniform base and a model photodegradable base on the photoacid reaction-diffusion process, TOA was added only to the MADMA receiving layer as illustrated in Figure 7. This strategy was used due to fix the base chemistry while examining the role of the base, because basicity, base size, and hydrophilicity also lead to complex changes in photoresist imaging.

An increased TOA concentration in the photobase case decreases the propagation depth of the reaction front and yields a sharper interface between protected and deprotected MADMA as shown in Figure 9. One important difference between this case and the uniform base case is that the deprotection near the acid feeder interface is not dependent upon the TOA concentration. Increasing the diffusion length of the photoacid through increased PEB time, increases the breath of the reaction front, but for concentrations greater than 0.2 %, the interface is much sharper for this case of the model photobase than the uniform base.

3.3 Roughness after development

The latent image profile characteristics are correlated to the image quality after development as shown by lithographic exposure aerial image quality¹⁵ and image-fading techniques¹⁶. The LER and relationship to the optical image quality can be quantified using the image-log slope (ILS) [3]. As the ILS increases, an improvement in LER results due to the sharper latent image. However, a plateau effect in LER was observed beyond $ILS = 15 \mu\text{m}^{-1}$. In comparison to the present model experiments, an ILS of order (600 to 1000) μm^{-1} is calculated, since interfacial width varies between (2 to 3) nm. Hence, this profile is degraded via photoacid reaction-diffusion permitting a focused discussion on the materials process effects, rather than optical image quality. We now discuss the effect of base on the relationship between the profile shape quantified as the latent-image log-slope and the surface roughness.

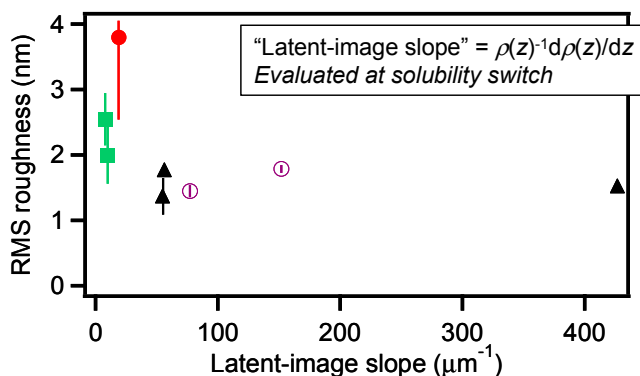


Figure 10. RMS roughness of developed bilayers as measured by AFM for different base locations: (●) no base, (■) coupled acid-base, (▲) uniform base, (○) model photobase. As the latent image slope increases, there is an improvement in the RMS roughness to a finite limit of approximately 1.5 nm [40].

Development of the bilayers with 0.26 N TMAH dissolves the top PHS acid feeder as well as some of the partially deprotected PMAAdMA. The solubility switch for this material is approximately 40 % deprotection – thus chains with greater than this fraction deprotection are soluble in the developer and are removed, while chains with a lesser degree of deprotection are insoluble. Based upon the geometry of the bilayer, the developed surface is analogous to the edge of a developed line. The surface roughness does not change dramatically for either the uniform or model photobase cases. However, these are less than the roughness found for the bilayer without base or when using the coupled acid-base bilayer.

Considering the LER dependence on initial image quality, it is surprising that the shape of the deprotection profile does not significantly influence LER. However, the initial ILS is extremely high, thus the subsequent reaction-diffusion might be insufficient to degrade the image quality to the point where an increase in LER is observed. Because the real-space deprotection profiles are available, we can define a metric analogous to ILS, which defines the optical image quality, for the deprotection profile shape; the latent-image slope. The latent-image slope is defined as the slope in the deprotection profile between deprotection extents of reaction of 0.35 and 0.5. Because the exposure dose remains constant in these experiments, the latent-image slope is truly analogous to ILS. Figure 10 illustrates the influence of latent-image slope on the developed roughness of the bilayer in terms of the RMS roughness. At low latent-image slope ($< 20 \mu\text{m}^{-1}$), there is an increase in the roughness of the developed bilayers similar to the increase in LER observed lithographically for $ILS < 15 \mu\text{m}^{-1}$. At larger latent-image slope, a plateau in the roughness is found with a limiting value of approximately 1.5 nm.

Thus, the limit in surface roughness is not solely due to the blur from the reaction-diffusion process. This result means that sharpening the deprotection front will only improve LER to its limiting value. However, because the model photobase results in a sharper deprotection profile than obtained for the uniform base at identical processing conditions, a photodegradable base should allow for high quality features to be printed at lower ILS than can be used for a typical base in lithographic processing. The

latent-image slope data suggest that strategies focused on another processing step such as development may be needed for any additional improvement in surface roughness beyond those that control the deprotection profile shape.

5. Conclusion

Identifying the intrinsic limits of chemically amplified photoresists is a critical challenge needed by the semiconductor industry to determine if new materials need to be developed or new imaging technologies are required. We systematically investigated each process step of the lithographic process to determine the contribution of each step and chemical species on roughness. The deprotection profiles from these cases were determined using a combination of neutron reflectivity and FTIR. We found that variations in processing conditions and molecular details influence strongly the profile of the reaction-diffusion front. The influence of a model base quencher, trioctylamine, on the deprotection front profile was determined through systematic variation of the base location. Base in the acid feeder layer ('exposed' regions) leads to a decrease in the level of deprotection near the initial line edge and broadens the deprotection front profile. Conversely, base in the MAdMA layer ('unexposed' regions) leads to a sharper deprotection front profile and decreases the propagation of the reaction front. In general, a sharper deprotection front leads to an improvement in the developed surface roughness of the bilayers to a limit of 1.5 nm. The model photodegradable base provides a sharper deprotection front than that obtained for the uniform base at identical processing conditions. Thus, it is probable that use of photodegradable bases would lower LER, based on the latent image quality improvement. The systematic study provides insight on how to reduce LER by not only by quenching acid that diffuses into unexposed regions, but by enhancing the deprotection extent at the line-edge that suppresses acid diffusion. This molecular mechanism can be accomplished with photodegradable bases to reduce LER by controlling the deprotection profile. However, the concept of adding excessive base for a sharper profile does not lower the roughness based upon a mechanism of narrow latent image profile. Nevertheless, identification of photoresist swelling at the line-edge suggests that the final roughness of the structure is controlled by the drying process during development. With this information, there are potential strategies to limiting LER by controlling the response of the photoresist to the developer solution.

6. Acknowledgements

This work would not have been possible without the tremendous contributions of members of the NIST photoresist project team: Bryan D. Vogt, Shuhui Kang, Ashwin Rao, David L. VanderHart, Sushil Satija, Sharadha Sambasiva, and Daniel A. Fischer. We are also thankful for many helpful discussions and support from Karen Turnquest, Kim Dean (SEMATECH), Ralph Dammel, Frank Houlihan, M. Padmanaban (AZ Electronics Materials), Jim Sounik, Michael Sheehan (DuPont Electronic Technologies), Tom Wallow (AMD), and Bill Hinsberg, Frances Houle, Hiroshi Ito (IBM). We also gratefully thank SEMATECH and the NIST Office of Microelectronics Programs (Steven Knight) for financial support for this work.

7. References

1. He, D.; Cerrina, F., *J Vac Sci Techn B* **1998**, 16 (6), 3748-3751.
2. Hinsberg, W.; Houle, F. A.; Hoffnagle, J.; Sanchez, M.; Wallraff, G.; Morrison, M.; Frank, S., *J Vac Sci Techn B* **1998**, 16, 3689-3694.
3. Pawloski, A.; Acheta, A.; Levinson, H.; Michaelson, T. B.; Jamieson, A.; Nishimura, Y.; Willson, C. G., *J. Microlith. , Microfab. , Microsyst.* **2006**, 5 (2), 023001-1-023001-16.
4. Shin, J.; Han, G.; Ma, Y.; Moloni, K.; Cerrina, F., *J Vac Sci Techn B* **2001**, 19 (6), 2890-2895.
5. Reynolds, G. W.; Taylor, J. W., *J Vac Sci Techn B* **1999**, 17 (2), 334-344.
6. Shin, J.; Ma, Y.; Cerrina, F., *J Vac Sci Techn B* **2002**, 20 (6), 2927-2931.
7. Houle, F. A.; Hinsberg, W. D.; Sanchez, M. I. *Macromolecules* **2002**, 35, 8591-8600.

8. Houle, F. A.; Hinsberg, W. D.; Sanchez, M. I. *Journal of Vacuum Science & Technology B* **2004**, 22 (2), 747-757.
9. Tsiartas, P. C.; Flanagan, L. W.; Henderson, C. L.; Hinsberg, W. D.; Sanchez, I. C.; Bonnacaze, R. T.; Willson, C. G. *Macromolecules* **1997**, 30 (16), 4656-4664.
10. Ito, H. *Journal of Polymer Science Part A-Polymer Chemistry* **2003**, 41 (24), 3863-3870.
11. Willson, C.; Ito, H.; Frechet, J.; Tessier, T.; Houliham, F. *Journal of the Electrochemical Society* **1986**, vol.133, no.1, 181-187.
12. Ito, H. *Adv Polym Sci* **2005**, 172, 37-245.
13. Wallraff, G. M.; Hinsberg, W. D. *Chem. Rev.* **1999**, 99, 1801-1821.
14. Houle, F. A.; Hinsberg, W. D.; Sanchez, M. I.; Hoffnagle, J. A. *Journal of Vacuum Science & Technology B* **2002**, 20 (3), 924-931.
15. Kim, J. H.; Kim, Y. H.; Chon, S. M.; Nagai, T.; Noda, M.; Yamaguchi, Y.; Makita, Y.; Nemoto, H. *Journal of Photopolymer Science and Technology* **2004**, 17 (3), 379-384.
16. Schmid, G. M.; Stewart, M. D.; Singh, V. K.; Willson, C. G. *J Vac Sci Techn B* **2002**, 20 (1), 185-190.
17. Stewart, M. D.; Tran, H. V.; Schmid, G. M.; Stachowiak, T. B.; Becker, D. J.; Willson, C. G. *Journal of Vacuum Science & Technology B* **2002**, 20 (6), 2946-2952.
18. Hoffnagle, J. A.; Hinsberg, W. D.; Sanchez, M. I.; Houle, F. A. *Optics Letters* **2002**, 27 (20), 1776-1778.
19. International Technology Roadmap for Semiconductors;2004 Update; 04.
20. Oertel, H. K.; Weiss, M.; Dammel, R.; Theis, J. *Microelectronic Engineering* **1990**, 11 (1-4), 267-270.
21. Yeh, T. F.; Shih, H. Y.; Reiser, A. *Macromol.* **1992**, 25 (20), 5345-5352.
22. Yeh, T. F.; Reiser, A.; Dammel, R. R.; Pawlowski, G.; Roeschert, H. *Macromol.* **1993**, 26 (15), 3862-3869.
23. Hunek, B.; Cussler, E. *AIChE Journal* **2003**, 48, 661-672.
24. Tsiartas, P. C.; Flanagan, L. W.; Hinsberg, W. D.; Henderson, C. L.; Sanchez, I. C.; Bonnacaze, R. T.; Willson, C. G. *Macromol.* **1997**, 30, 4656-4664.
25. Burns, S. D.; Schmid, G. M.; Tsiartas, P. C.; Willson, C. G.; Flanagan, L. *Journal of Vacuum Science & Technology B* **2002**, 20 (2), 537-543.
26. Hinsberg, W.; Houle, F. A.; Lee, S. W.; Ito, H.; Kanazawa, K. *Macromol.* **2005**, 38 (5), 1882-1898.
27. Houle, F. A.; Hinsberg, W. D.; Sanchez, M. I. *Macromol.* **2002**, 35 (22), 8591-8600.
28. Ito, H.; Wallraff, G. M.; Fender, N.; Brock, P. J.; Hinsberg, W. D.; Mahorowala, A.; Larson, C. E.; Truong, H. D.; Breyta, G.; Allen, R. D. *Journal of Vacuum Science & Technology B* **2001**, 19 (6), 2678-2684.
29. Ito, H.; Hinsberg, W. D.; Rhodes, L.; Chang, C. *Proceedings of the SPIE, Advances in Resist Technology and Processing XX* **2003**, 5039, 70-79.
30. Prabhu, V. M.; Vogt, B. D.; Wu, W. L.; Douglas, J. F.; Lin, E. K.; Satija, S. K.; Goldfarb, D. L.; Ito, H. *Langmuir* **2005**, 21 (15), 6647-6651.
31. Ito, H.; Allen, R. D.; Opitz, J.; Wallow, T. I.; Troung, H. D.; Hofer, D. C.; Varansai, P. R.; Jordhamo, G. M.; Jayaraman, S.; Vicari, R. *Proceedings of the SPIE, Advances in Resist Technology and Processing XVII* **2000**, 3999, 2-12.
32. Prabhu, V. M.; Rao, A. B.; Kang, S.; Lavery, K. A.; Lin, E. K.; Satija, S. K.; *Proceedings of the SPIE, Advances in Resist Technology and Processing XXIV* **2007**, 6519, submitted.
33. Hinsberg, W. D.; Houle, F. A.; Sanchez, M. I.; Wallraff, G. M. *IBM Journal of Research and Development* **2001**, 45 (5), 667-682.
34. Houle, F. A.; Hinsberg, W. D.; Morrison, M.; Sanchez, M. I.; Wallraff, G.; Larson, C.; Hoffnagle, J. *J Vac Sci Techn B* **2000**, 18 (4), 1874-1885.

35. Lin, E. K.; Soles, C. L.; Goldfarb, D. L.; Trinqué, B. C.; Burns, S. D.; Jones, R. L.; Lenhart, J. L.; Angelopoulos, M.; Willson, C. G.; Satija, S. K.; Wu, W. L. *Science* **2002**, 297, 372-375.
36. Kang, S.; Prabhu, V. M.; Vogt, B. D.; Lin, E. K.; Wu, W. L.; Turnquest, K. *Proceedings of the SPIE - The International Society for Optical Engineering* **2006**, 6153, 61533N.
37. Postnikov, S. V.; Stewart, M. D.; Tran, H. V.; Nierode, M. A.; Medeiros, D. R.; Cao, T.; Byers, J.; Webber, S. E.; Wilson, C. G. *Journal of Vacuum Science & Technology B* **1999**, 17 (6), 3335-3338.
38. Kang, S.; Prabhu, V. M.; Vogt, B. D.; Lin, E. K.; Wu, W. L.; Turnquest, K. *Polymer* **2006**, 47 (18), 6293-6302.
39. Vogt, B. D.; Kang, S.; Prabhu, V. M.; Lin, E.K.; Satija, S.K.; Turnquest, K.; Wu, W. L. *Macromolecules* **2006** 39, 8311-8317.
40. Vogt, B. D.; Kang, S.; Prabhu, V. M.; Rao, A. B.; Lin, E.K.; Satija, S.K.; Turnquest, K.; Wu, W. L. *Journal of Vacuum Science and Technology B* **2007** 25,175-182.